Nanomed Res J 4(3):193-203, Summer 2019

RESEARCH ARTICLE

Synthesis and Characterization of a Novel Fe_3O_4-SiO_2@Gold Core-Shell Biocompatible Magnetic Nanoparticles for Biological and Medical Applications

Meisam Sadeghi[1,*], Mohsen Jahanshahi[1], Hamedreza Javadian[2]

[1] *Nanotechnology Research Institute, Faculty of Chemical Engineering, Babol Noushirvani University of Technology, Babol, Iran*

[2] *Universitat Politècnica de Catalunya, Department of Chemical Engineering, ETSEIB, Diagonal 647, 08028 Barcelona, Spain*

ARTICLE INFO

Article History:
Received 19 May 2019
Accepted 21 August 2019
Published 15 September 2019

Keywords:
Bagg Albino/C Mice
Biocompatible Magnetic Nanoparticles
Biological And Medical Applications
Core-Shell Sio_2-Fe_3O_4@Gold
Muscle Cancer Model

ABSTRACT

Objectives: In this study, an efficient and fast method has been developed for synthesis of a novel magnetite nanoparticles Fe_3O_4@SiO_2@Gold as an efficient boronated nanodrug carrier. Application and characterization of core-shell iron oxide (Fe_3O_4/γ-Fe_2O_3) magnetic nanoparticles (MNPs) with an inner silica shell and outer of Gold shell (Fe_3O_4-SiO_2@Gold (FSG)) in Boron Neutrons Capture Therapy (BNCT) highlighted. The main problem dealing with cancer cells is that the tumor and normal cells ones are mixed without a map of the boron accumulation.

Methods: The content of the discussion include the possibility of a FSG mediated by liposome as the boron carriers for the transfer of boron compound to tumor tissue. Furthermore, folate receptor was considered as an appropriate substrate that has great potential to attach to tumor. The present work aimed to study boron biodistribution in the muscle cancer animal model in Bagg Albino (BALB/c) mice employing PEGylated liposome-encapsulated FSG formulations.

Results: The predetermined boron concentration was obtained to be 20-35 mg ^{10}B/g. Samples of the tumor tissue, such as kidney, liver, lung, heart, skin, spleen, brain, stomach, and bone were taken as post-administration at different times to measure boron content by Inductively Coupled Plasma (ICP) analysis. The results showed the existence of GLUT-5 expression as an erythrocyte-type glucose transporter protein in a wide variety of tumor cells.

Conclusions: Fe_3O_4-SiO_2 nanoparticles are highly biocompatible with biological materials and also Gold shell exposes the magnetic properties.

How to cite this article
Sadeghi M, Jahanshahi M, Javadian HR. Synthesis and Characterization of a Novel Fe_3O_4-SiO_2@Gold Core-Shell Biocompatible Magnetic Nanoparticles for Biological and Medical Applications. Nanomed Res J, 2019; 4(3): 193-203.
DOI: 10.22034/nmrj.2019.03.008

INTRODUCTION

In the past decade, magnetic micro and nanoparticles have attracted much attention because of their unique magnetic properties and widespread application in different fields. Magnetic nanoparticles are efficient, and readily available, and have high surface-area resulting in high catalyst loading capacity [1], chemical sensing [2-6], information storage [7, 8] and medical diagnostics [9–11] and outstanding stability to heterogeneous supports for catalysts preparation. Accordingly, the application of magnetic nano particles has become an interesting filed of research besides other advantages of nano particles [12, 13]. A series of functionalized magnetic nanoparticles (MNPs) involves iron oxide (Fe_3O_4/γ-Fe_2O_3) magnetic nanoparticles coated with silica and Gold shells. [14]. Importantly, Core-shell nanoparticle provides both enhanced biocompatibility and stability of the surface and imparts the surfaces

* Corresponding Author Email: *meisam_sadeghi1363@yahoo.com*

with the desired biological or chemical, catalytic interfacial reactivities [15, 16]. The successes of these synthetic approaches discover the potential applications of FSG [17-20].

In pharmaceutical and medical aspects, novel drug delivery systems such as polymers, liposomes, and Monoclonal antibodies open new views in cancer treatment [21]. Traveling of Magnetic nanoparticles, such as Fe_3O_4-SiO_2 core-shell through the bloodstream and tendency to accumulate into the surrounding tumor tissue is important. [22]. One significant aspect is the development of compounds that can deliver a high boron payload to the tumors [23]. Hence, considerable successes have been obtained on the liposomal delivery system as a new targeting fact.

Liposomes are profitable drug delivery carriers that are able to selectively transfer a large amount of a broad variety of ^{10}B agents to the tumor tissue. For this purpose, for carrier system development, folate receptors was considered as an appropriate substrate that has a potential to attach to tumor compared with normal cells. During the investigation of its applicable behavior, we have found that the muscle cancer in BALB/c mice model possesses a unique advantage for treatment of tumors [24-27].

The main problem dealing with muscle cancer is that the tumor and normal cells are mixed without a map of the boron accumulation. As a result, in different tissue samples, the boron concentration in tissue composition is not accurate. The purpose of study was to perform biodistribution studies of FSG in the muscle cancer in BALB/c mice model. In this model, we have examined different sites surrounding healthy organs in the BALB/c mice model. The optimization of selective boron delivery to cancer cells is an interesting area of research and must be as a starting point to contribute and optimize its therapeutic efficacy. Using a novel drug containing ^{10}B compound in smart release and administering to a patient is a novel method in the treatment of the cancerous tumors. The reduce production cost as well as minimum side effects in treatment are other advantages of the applied drug and method.

In the present article, 41.1 mg of the liposome-encapsulated FSG was delivered to a tumor site. Results demonstrated that the highest concentration of drug in the tumor tissue (27 mg/L) occurs at a period of 45 min to 3 h. Hence, Specific method of inductively coupled plasma (ICP) analysis was applied for samples of the tumor, normal (muscle) tissue, liver, heart, lung, spleen, skin, stomach, brain, bone, kidney and blood to check the boron distribution in different tissue portions.

MATERIALS AND METHODS

Preparation of Fe_3O_4-SiO_2@Gold (FSG) nanoparticles

Preparation of the Fe_3O_4 nanoparticles (FMNs)

Fe_3O_4 nanoparticles were synthesized using a modified protocol. $FeCl_3$ and $FeCl_2$ solution in HCl with the optimum mole fraction ratio of Fe^{3+}: Fe^{2+} in 2:1 (Fig. 1) was added to a flat bottom balloon separately and stirred using a magnetic stirring bar.

To prepare water-soluble and dispersed FMNs, the solutions of $FeCl_3.6H_2O$ (1 M) and $FeCl_2.4H_2O$ (2 M) were prepared by dissolving the iron salts in 2 and 1 M HCl solutions in a 250 ml flask. Then, the solutions were mixed at 25 °C. Then, ammonia solution (1 M, 100 ml) was added droplet. Then, particles were filtered and washed several times. The pH of the solution was adjusted up to 10. The stirring of the solution was continued for 1 h until the stable black FMNs were appeared. The ferrite powder was finally dried in vacuum oven at 80 °C for 24 h to complete removal of water. The reaction mechanism is explained as below.

$$Fe^{2+} + 2Fe^{+} + 8NH_3 + H_2O \rightarrow Fe_3O_4 + NH_4OH$$

Preparation of the Fe_3O_4/SiO_2 magnetic nanoparticles (FSMNs)

The core/shell Fe_3O_4@SiO_2 was prepared according to the Stober process [28] with some modifications. The obtained MNPs powder (1g) were dispersed in a mixture of 100 mL of ethanol,

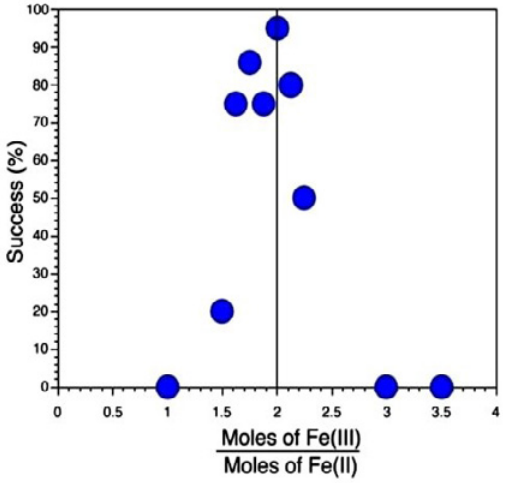

Fig. 1. Optimization of Fe^{3+} / Fe^{2+} ratio for production of Fe_3O_4

20 mL of distilled water by the ultrasonic treatment for 30 min and 5.0 mL of 28 wt % concentrated ammonia aqueous solution ($NH_3.3H_2O$) with vigorous stirring, followed by the addition of 2 mL of Tetra Ethyl Ortho Silicate (TEOS) was dropwise added to this dispersion. The resulting dispersion was kept stirred mechanically under N_2 protection for 12 h at room temperature. The obtained Fe_3O_4@ SiO_2 nanoparticles were separated with a magnet and washed repeatedly with ethanol and water to remove nonmagnetic byproduct.

Activation of FSMNs

Then, the obtained MNPs powder (1g) was dispersed in methanol (100 mL) and toluene (30 mL) by the ultrasonic treatment for 30 min before 3-Amino Propyl Tri Ethoxy Silane (APTES), (99%, 1 mL) was added to the mixture. After mechanically agitation for 12 h, the suspended substance was separated by a magnet. The settlement product was redispersed in ethanol by sonication and isolated with magnetic decantation for 5 times. The precipitated product (APTES-MNPs) was dried at room temperature under vacuum. The reactions mechanism is explained as below.

$$FeCl_2 + 2FeCl_3 + 8NH_4OH \rightarrow Fe_3O_4 + 8NH_4Cl + 4H_2O$$

$$Fe_3O_4.nCl^- + mH_2O \rightarrow Fe_3O_4 mOH^- + nCl^- + mH^+$$

$$Si(OC_2H_5) + H_2O \rightarrow Si(OH)_4 + C_2H_5OH$$

Preparation of Fe_3O_4-SiO_2@Gold nanoparticles

The synthesis of Fe_3O_4 nanoparticles starts according to process in which $Fe(acac)_3$ is reduced using 1,2-hexadecanediol in the presence of oleic acid. Following Fe_3O_4 make as nanoparticles with the favorite sizes, Gold is deposited on to the surface of Fe_3O_4 by reduction of $Au(CH_3COO)_3$ using 1,2-hexadecanediol in the presence of oleic acid at higher temperature (180–190 °C). The resulting Fe_3O_4-SiO_2@Gold nanoparticles can be separated by centrifugation from the uncoated Fe_3O_4 nanoparticles.

This approach can produce highly monodisperse Fe-oxide-SiO_2-Gold nanoparticles.

Synthetic procedure of liposome-encapsulated FSG

The synthetic procedure of liposome-encapsulated FSG using polyethylene glycol (PEG) as a precursor mentioned in the literature [29] allows a solubility of the drug in the blood and binding of a ligand to the liposome. Furthermore, folate ligand bonded to the PEG. As demonstrated in Fig. 3, the liposome can encapsulate aqueous solutions of sodium salts anions and join lipophilic boron-containing nanodrug components embedded within the bilayer membrane [30]. For this purpose, 1 M solution of fructose in water or ethanol and 1 M solution of boric acid containing ^{10}Boron were provided. Also, adjusting and controlling the solution pH around 3-4 was performed. Then, some carbonate salt of solid calcium (dissolved in a little amount of deionized water) was added to the solution. As a result of this process, the biphasic solution was formed and the lower phase was separated. Nanodrug has several boron atoms in each molecule that caused to easily penetrate to the membrane of the tumor cell.

Model of cancer: Biodistribution and boron analysis studies

The digestion of animals samples was carried out according procedure as discussed in the

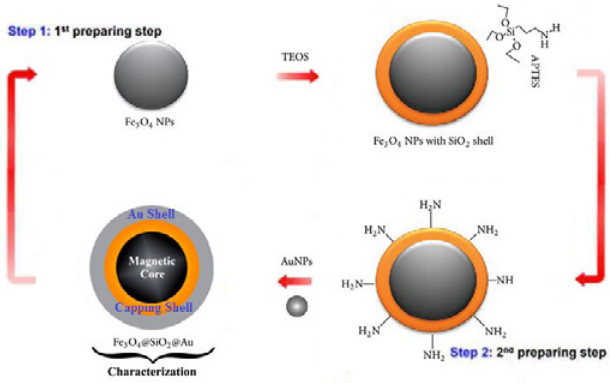

Fig. 2. Step 1: An illustration of the Fe_3O_4 magnetic nanoparticles and synthesis of the Fe_3O_4-SiO_2 magnetic nanoparticles. Step 2: Schematic process of producing the core – shell Fe_3O_4-SiO_2@Gold nanoparticles

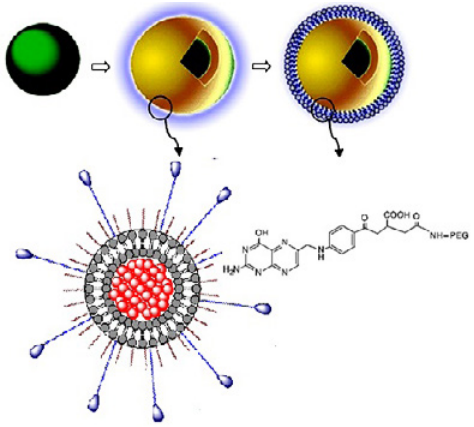

Fig. 3. Schematic of liposome-encapsulated FSG

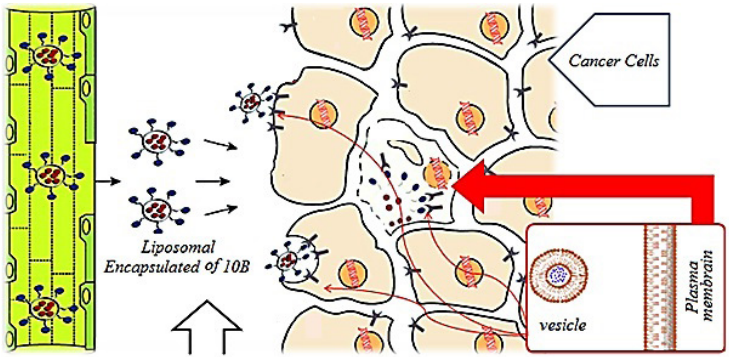

Fig. 4. Overall schematic of the nanodrug entrance into the blood and tissue

literature [31]. Over time, to identify the optimal injection protocol for delivery of boron to the tumor tissue, performed experiments were analyzed. Following the appropriate experiments, the data were presented and boron concentration was individually analyzed.

In the present study, several samples of tumor and cancerous tissues around tumor tissues were taken from each animal to informant the distribution of boron in the tumor, blood, and normal tissues [32]. Boron concentration values in the tumor, blood, and normal (muscle) tissues were obtained as post-administration to calculate the ratio of boron concentration in tumor/blood, normal tissue/blood and tumor/normal tissue for each of the compounds [33]. Fig. 4 shows an overall schematic of the entrance process of the drug and the process of BNCT used in the prior investigation.

RESULTS AND DISCUSSION

In order to investigate the morphology and the structure of FSG nanoparticle, the prepared particles were analyzed.

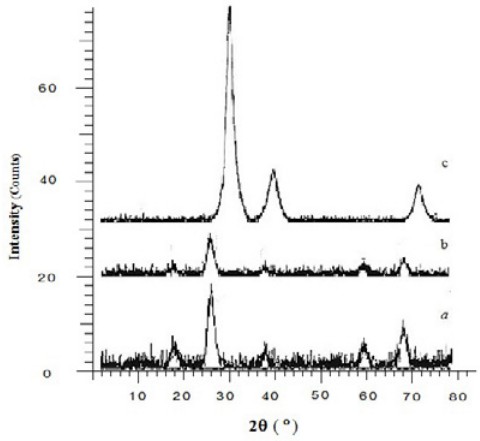

Fig. 5. X-ray diffraction pattern for the (*a*) Fe_3O_4 nanoparticles (b) Fe_3O_4-SiO_2 nanoparticles (c) Fe_3O_4-SiO_2@Gold nanoparticles

Qualitative and Quantitative Analysis

XRD *analysis of FSG nanoparticles*

X-ray diffraction pattern (JCPDS, card number 01-072-1243) for the (*a*) Fe_3O_4 nanoparticles (b) Fe_3O_4-SiO_2 nanoparticles (c) Fe_3O_4-SiO_2@Gold

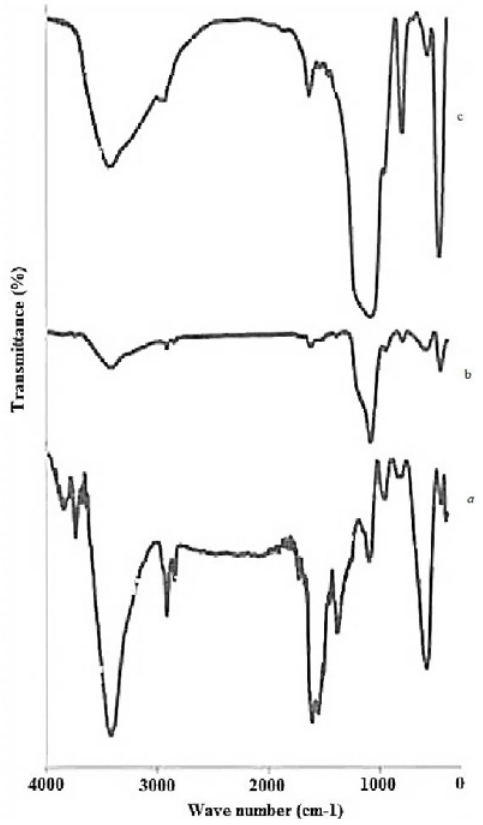

Fig. 6. The FTIR spectra of (*a*) Fe_3O_4 nanoparticles (b) Fe_3O_4-SiO_2 nanoparticles (c) Fe_3O_4-SiO_2@Gold nanoparticles

nanoparticles showed in Fig. 5. The XRD pattern showed the characteristic peaks at 2θ of 9.2◦, 11◦, 31.8◦, and 45.4◦ and the size of Fe_3O_4 nanoparticles obtained was 9.80 nm. Furthermore, the data showed diffraction peaks at 2θ° = 38.2°, 44.2°, 64.5°, 77.8°, and 81.7°, which can be indexed to planes of Gold.

FTIR *analysis of FSG nanoparticles*

The reactions were confirmed using the FTIR analysis. The FTIR spectra of (*a*) Fe_3O_4 nanoparticles (*b*) Fe_3O_4-SiO_2 nanoparticles and (c) Fe_3O_4-SiO_2@ Gold nanoparticles showed in Fig. 6. In contrast to the spectrum of Fe_3O_4-SiO_2 nanoparticles, the spectrum of the Fe_3O_4-SiO_2@Gold nanoparticles shows a bond at 3400 cm^{-1}, that could be assigned to N-H stretching. The bonds at 1020 cm^{-1} also could be attributed to the stretching of C-H groups of alkyls in the Fe_3O_4-SiO_2@Gold nanoparticles. The magnetite spectrum shows a bond at 573 cm^{-1}, that could be assigned to magnetite vibrations. The bonds at 3440 cm^{-1} also could be attributed to the stretching of O-H groups of hydroxyls in the magnetic nanoparticles. Furthermore, the bonds at 1614 and 1391 cm^{-1} that appeared in the spectrum of the Fe_3O_4-SiO_2 nanoparticles could be attributed to formation of carboxyl group bond to Fe_3O_4 in Fe_3O_4-SiO_2 nanoparticles. In addition, the bonds

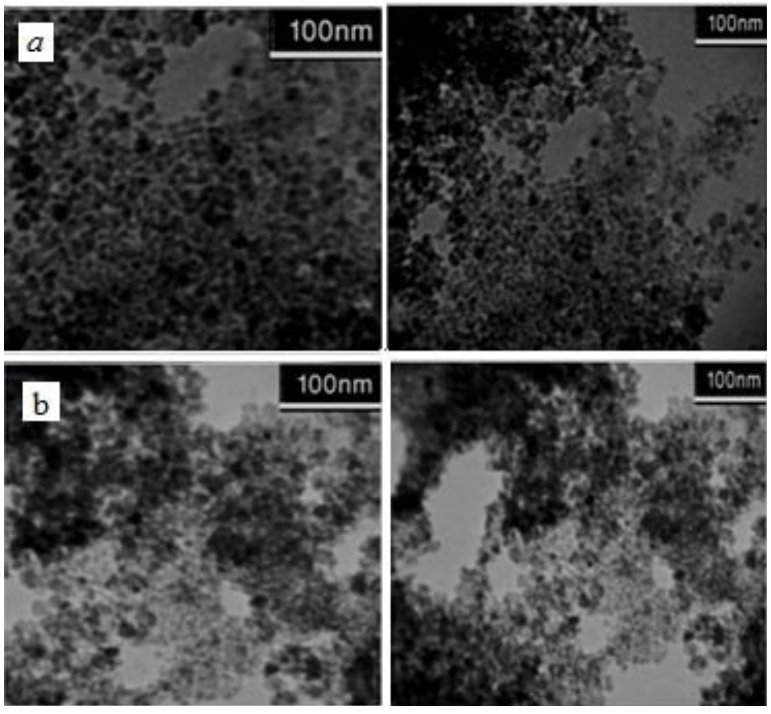

Fig. 7. The TEM image of (*a*) Fe_3O_4-SiO_2@Gold nanoparticles and (b) Fe_3O_4-SiO_2 nanoparticles

at 1621, 1091 and 955 cm^{-1} could be attributed to H-O-H stretching, Si-O-Si stretching and Si-OH stretching in magnetite-silica nanoparticles.

TEM study of FSG nanoparticles

TEM data supports Fe_3O_4-SiO_2@Gold core shell nanoparticles forms. There are two major findings from the morphological comparison. Firstly, the particles after coating with Silica and Gold seem much darker and secondly, for the particles after coating with SiO_2 and Gold, the average particle size changed from 9.8 nm to 15 nm. In Fig. 6, the TEM data prepare an important piece of evidence for Fe_3O_4-SiO_2@Gold core-shell forms.

Biodistribution and boron analysis studies: in-vivo and in-vitro treatment

In this section, the experiments conducted which were related to *in-vivo* and *in-vitro* conditions of the biological tests. Studying the effects of drug-containing ^{10}B on the muscle cancer and the corresponding Dose-Responses curves were performed. The predetermined concentration was 20-35 mg $^{10}B/g$. The experiments were performed dealing with the biological distribution of the designed drug in different times of injection, biological distribution of various doses of the drug and sufficient accumulation of the designed drug-containing ^{10}Boron aiming influential treatment of the tumor.

As mentioned above, the drug with concentrations of 15, 25, 35 and 45 mg was selected to inject to the animal. The results of ICP data indicate that the drug concentration of 35 mg into the cell culture medium maximized the accumulation of the drug within 24 h incubation of the drug introduced to the environment (**Fig**. 8). The reason can be attributed to the representation of the toxicity of the synthesized composition using MTT assay method.

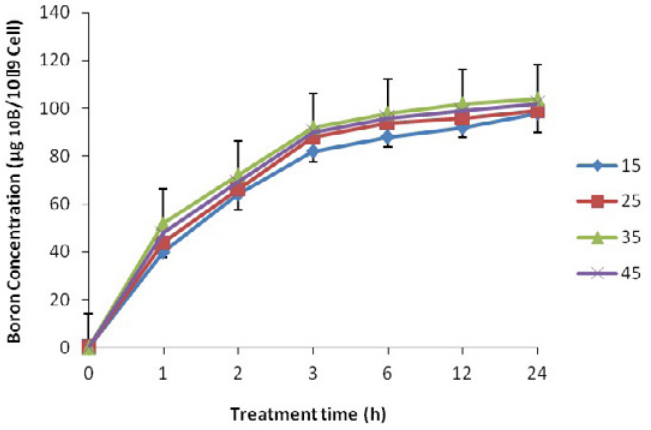

Fig. 8. Optimum boron concentrations (µg) vs treatment time, ICP for the drug

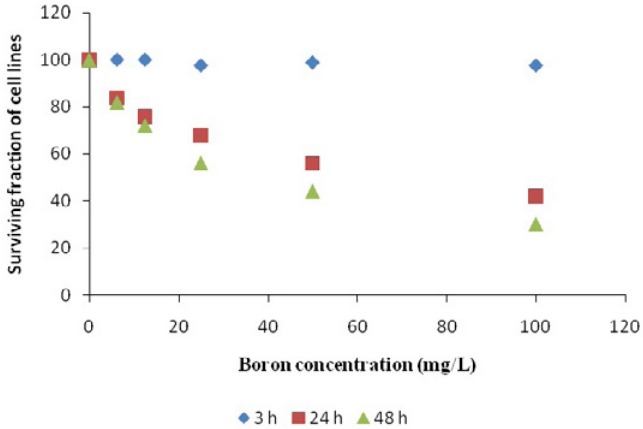

Fig. 9. Diagram of toxicity for in-vivo treatment in animal

To perform *in-vivo* treatment in testing animal, the toxicity of the liposome-encapsulated FSG was analyzed. Fig. 9 shows the diagram of toxicity of the liposome-encapsulated FSG determined by MTT assay method [34].

As can be seen, in the initial time, the number of live cells is not considerably changed; because of using the unit dietary compound to drug synthesis. While with respect to time, the number of tumor cells is gradually decreased. After 24 h, these reductions were 79, 64, 50, 80 and 36 % for various boron compounds at concentrations of 5, 10, 25, 50 and 100 mg/L, respectively. After 48 h, the results were similar to those obtained after 24 h with a slight differences [35].

Boron biodistribution studies were essential to preclinical design and subsequent clinical research protocols of BNCT. In particular, this analysis identifies the optimum time post-administration of the boron carrier to perform neutron therapy [36]. To date, dose calculations were based on boron content values in blood, tumor, and normal tissues obtained beforehand from biodistribution studies. in the case of animal models, calculations were based on the mean values obtained from biodistribution studies in separate portions of tissues [37]. The tabulated diagrams and data corresponding to the mean value ± standard deviation of the ratio for each sample are shown in Fig. 10.

The results showed that the highest concentration of drug in the tumor tissue occurred at a period of 45 min to 3 h. Also, after drug injection, its concentration initially in the blood reached to the highest value; while it may reach to the lowest value within 24 h [38].

Generally, the results of boron concentration in the tumor tissue showed that after 3 h of drug injection to the tumor, the drug concentration reached to its highest level (27 mg/L) due to the excessive amount of sugar transmitters such as GLUT5 in the tumor cells. It can be concluded that the transfer of FSG was carried out by the GLUT5 transmitter to the tumor [39]. Since, the number of these transmitters in the cancerous tissue is greater

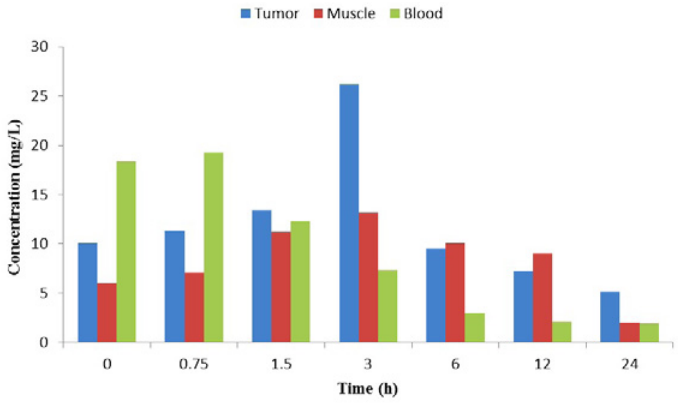

Fig. 10. Boron concentration in blood, normal tissue and tumor tissue for drug with respect to time

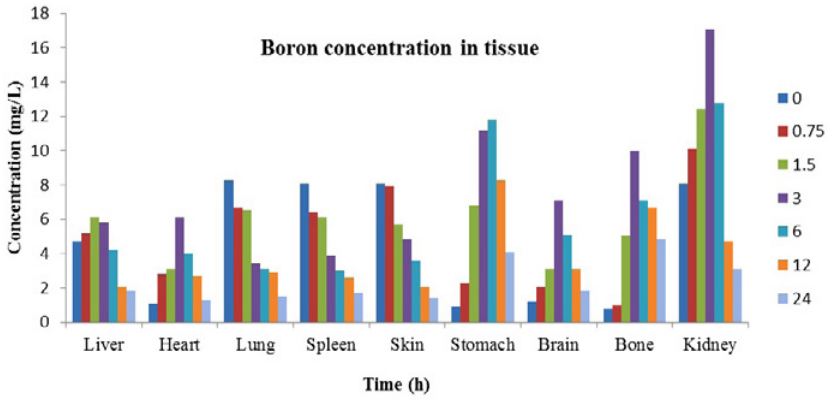

Fig. 11. Boron concentration in several tissue samples for the drug with respect to time (h)

Table 1. T/N, T/B, and N/B boron concentration ratios in mice administration FSG

Ratio	Time (h) after administration						
	0	0.75	1.5	3	6	12	24
T/N	0.33	0.37	0.91	1.81	3.37	4.29	1.05
T/B	0.55	0.59	1.09	3.59	3.17	3.43	2.69
N/B	1.68	1.59	1.20	1.98	0.94	0.80	2.55

T: Tumor; N: Normal tissue (muscle); B: Blood;

than other tissues, selective accumulation of drug in the cancerous tissue occurred.

The drug concentration in the tumor tissue increased with respect to time due to the drug release to the tumor tissue through the blood [40]. With the accumulation of drug in the tumor, its concentration increased after 6 h of injection due to the sugar consumption of the drug by tumor cells and then, the amount of boron in the tumor tissue reduced. These results were consistent with the results obtained by other researchers regarding the excessive amount of sugar transmitters in tumor tissue [41]. Furthermore, Table 1 shows the absolute boron concentration values for the blood, tumor and normal tissues. The boron concentration (BC) in the blood, compared with normal tissue, is often used as the cited phrase to calculate the BC in the tumor for BNCT. By injecting the drug, its concentration in the blood reached to the highest value at initial time, and by transferring drug to other tissues and organs at long duration of time, its concentration ultimately decreased and reached to the lowest level within 24 h after injection [42]. In this article, the ratio of BC in normal tissue to that in blood, i.e. N/B ratio, remains about ~1.6 at 45 min post-administration [43].

Fig. 11 shows a graphical representation of the biodistribution of the ^{10}B-drug in different tissues of the model of the animal body at different time, after injection (41.1 mg of ^{10}Boron complex per every 30 g of the animal weight). The concentration of boron in the kidneys tissue initially increased and reached to the highest value of 17 mg/L within 3 h after injection. The kidneys contain glomeruli that are blood filters. Hence, these data are consistent with the results of Edward's study that highlights the expression of GLUT5 in the kidney glomerular tissue. In liver tissue, the accumulation of the drug reached to the highest value. The results of the ICP analysis for heart tissue were similar to the results obtained for normal tissue due to the muscular structure of the heart. The results of drug distribution studies on spleen and lung tissues were interesting. Furthermore, the results show that the drug concentration was high at initial time after injection to the lung and spleen tissues due to the high rate of blood donation in the tissues. With respect to time, it is observed that the concentration of drug in the tissues significantly reduced and reached to its minimum value (2 mg/L) within 24 h. The concentration of the drug in the skin tissue at the initial time has reached to the highest value and then, rapidly reduced to 1.5 mg/L for duration of 3 h. This result can be attributed to the high distribution of blood capillary network inside the skin tissue [44]. At the initial time after injection, the concentration of boron in the skin tissue increased and then, decreased with respect to time with blood circulation. The study of drug concentration in stomach tissue shows its highest concentration after 3 and 6 h of injection and then, follows descending trend to the value of 4 mg/L within 24 h after injection. The reason for high concentrations of boron in the stomach tissue can be attributed to its muscle structure and high blood donation at a time interval of 3 to 6 h. The highest amount of boron in the brain tissue occurred within 3 h after injection. The concentration of boron in the bone tissue increased to 10 mg/L after 3 h with a high rate.

Considering high importance of the tissues in the case of breast cancer, it can be concluded that the mean concentration of boron considerably decreased and its value falls within the range of 6 to 10 mg/L, similarly for tumor, lung, spleen, and skin tissues.

CONCLUSIONS

There are many challenging issues for the application and characterization of the detailed core-shell FSG nanostructures. Results demonstrated that the coupling of the biological and catalytic interfacial reactivity and the magnetic activity of core-shell nanoparticles is an effort to further broaden the rapidly-emerging field of core@shell magnetic. In this study, the time-course biodistribution of boron delivered by liposome-encapsulated FSG in the BALB/c

mice muscle cancer model was reported for the first time. In summary, it was demonstrated that the combined administration of FSG offers the most similarity in practicable targeting of different tumors; because of these boron carriers have different uptake mechanisms and properties. Furthermore, it was possible to selectively transfer the amounts of therapeutic boron to BALB/c mice tumor and achieve ratios between tumor and blood that was compatible with the treatment. The results of ICP data indicated that the drug concentration of 35 mg in the cell culture medium maximized the accumulation of the drug for 24 h incubation after the drug introduced to the environment. Also, the highest concentration of drug (27 mg/L) in the tumor tissue occurs at a period of 45 min to 3 h due to the excessive amount of sugar transmitters such as GLUT5 in the tumor cells. In summary, the results of the present study demonstrated that the therapeutic potential of boron-bearing liposomes led to large boron biodistribution values [45-50]. The results can be considered as a guideline for further understanding boron targeting processes associated with the agents studied.

ACKNOWLEDGEMENTS

The authors gratefully acknowledge the staffs of University of Isfahan, central laboratory in Isfahan University of Technology and Nano Technology Department, Agricultural Biotechnology Research Institute of Iran for their assistance on this research.

CONFLICT OF INTEREST

The authors declare that there are no conflicts of interest regarding the publication of this manuscript.

REFERENCES

1. Fan R, Min H, Hong X, Yi Q, Liu W, Zhang Q, et al. Plant tannin immobilized Fe3O4@SiO2 microspheres: A novel and green magnetic bio-sorbent with superior adsorption capacities for gold and palladium. Journal of Hazardous Materials. 2019;364:780-90.
2. Mohammad-Beigi H, Yaghmaei S, Roostaazad R, Arpanaei A. Comparison of different strategies for the assembly of gold colloids onto Fe3O4@SiO2 nanocomposite particles. Physica E: Low-dimensional Systems and Nanostructures. 2013;49:30-8.
3. Khosroshahi ME, Ghazanfari L. Physicochemical characterization of Fe3O4/SiO2/Au multilayer nanostructure. Materials Chemistry and Physics. 2012;133(1):55-62.
4. Zhang Y, Xu Q, Zhang S, Liu J, Zhou J, Xu H, et al. Preparation of thiol-modified Fe3O4@SiO2 nanoparticles and their application for gold recovery from dilute solution. Separation and Purification Technology. 2013;116:391-7.
5. Chen X, Zhu J, Chen Z, Xu C, Wang Y, Yao C. A novel bienzyme glucose biosensor based on three-layer Au–Fe3O4@SiO2 magnetic nanocomposite. Sensors and Actuators B: Chemical. 2011;159(1):220-8.
6. Yang L, Li N, Wang K, Hai X, Liu J, Dang F. A novel peptide/Fe3O4@SiO2-Au nanocomposite-based fluorescence biosensor for the highly selective and sensitive detection of prostate-specific antigen. Talanta. 2018;179:531-7.
7. Chen J, Pang S, He L, Nugen SR. Highly sensitive and selective detection of nitrite ions using Fe3O4@SiO2/Au magnetic nanoparticles by surface-enhanced Raman spectroscopy. Biosensors and Bioelectronics. 2016;85:726-33.
8. Luo S, Liu Y, Rao H, Wang Y, Wang X. Fluorescence and magnetic nanocomposite Fe 3 O 4 @SiO 2 @Au MNPs as peroxidase mimetics for glucose detection. Analytical Biochemistry. 2017;538:26-33.
9. Amatatongchai M, Sitanurak J, Sroysee W, Sodanat S, Chairam S, Jarujamrus P, et al. Highly sensitive and selective electrochemical paper-based device using a graphite screen-printed electrode modified with molecularly imprinted polymers coated Fe3O4@Au@SiO2 for serotonin determination. Analytica Chimica Acta. 2019;1077:255-65.
10. Farimani MHR, Shahtahmasebi N, Rezaee Roknabadi M, Ghows N, Kazemi A. Study of structural and magnetic properties of superparamagnetic Fe3O4/SiO2 core–shell nanocomposites synthesized with hydrophilic citrate-modified Fe3O4 seeds via a sol–gel approach. Physica E: Low-dimensional Systems and Nanostructures. 2013;53:207-16.
11. Ma J, Sun N, Wang C, Xue J, Qiang L. Facile synthesis of novel Fe3O4@SiO2@mSiO2@TiO2 core-shell microspheres with mesoporous structure and their photocatalytic performance. Journal of Alloys and Compounds. 2018;743:456-63.
12. Fu X, Liu J, He X. A facile preparation method for single-hole hollow Fe3O4@SiO2 microspheres. Colloids and Surfaces A: Physicochemical and Engineering Aspects. 2014;453:101-8.
13. Kashanian F, Kokkinis G, Bernardi J, Zand MR, Shamloo A, Giouroudi I. A novel magnetic microfluidic platform for on-chip separation of 3 types of silica coated magnetic nanoparticles (Fe3O4@SiO2). Sensors and Actuators A: Physical. 2018;270:223-30.
14. Roto R, Yusran Y, Kuncaka A. Magnetic adsorbent of Fe 3 O 4 @SiO 2 core-shell nanoparticles modified with thiol group for chloroauric ion adsorption. Applied Surface Science. 2016;377:30-6.
15. Zhou J, Gan N, Li T, Zhou H, Li X, Cao Y, et al. Ultratrace detection of C-reactive protein by a piezoelectric immunosensor based on Fe3O4@SiO2 magnetic capture nanoprobes and HRP-antibody co-immobilized nano gold as signal tags. Sensors and Actuators B: Chemical. 2013;178:494-500.
16. Shi L, Huang J, He Y. Recyclable purification-evaporation systems based on Fe 3 O 4 @TiO 2 nanoparticles. Energy Procedia. 2017;142:356-61.
17. Cîrcu M, Radu T, Porav AS, Turcu R. Surface functionalization of Fe3O4@SiO2 core-shell

nanoparticles with vinylimidazole-rare earth complexes: Synthesis, physico-chemical properties and protein interaction effects. Applied Surface Science. 2018;453:457-63.
18. Veera Manohara Reddy Y, Sravani B, Agarwal S, Gupta VK, Madhavi G. Electrochemical sensor for detection of uric acid in the presence of ascorbic acid and dopamine using the poly(DPA)/SiO 2 @Fe 3 O 4 modified carbon paste electrode. Journal of Electroanalytical Chemistry. 2018;820:168-75.
19. Veisi H, Razeghi S, Mohammadi P, Hemmati S. Silver nanoparticles decorated on thiol-modified magnetite nanoparticles (Fe3O4/SiO2-Pr-S-Ag) as a recyclable nanocatalyst for degradation of organic dyes. Materials Science and Engineering: C. 2019;97:624-31.
20. Mir N, Karimi P, Castano CE, Norouzi N, Rojas JV, Mohammadi R. Functionalizing Fe3O4@SiO2 with a novel mercaptobenzothiazole derivative: Application to trace fluorometric and colorimetric detection of Fe3+ in water. Applied Surface Science. 2019;487:876-88.
21. Jie G, Ge J, Gao X, Li C. Amplified electrochem-iluminescence detection of CEA based on magnetic Fe3O4@Au nanoparticles-assembled Ru@SiO2 nanocomposites combined with multiple cycling amplification strategy. Biosensors and Bioelectronics. 2018;118:115-21.
22. Ma Y, Mu B, Zhang X, Zhang H, Xu H, Qu Z, et al. Hierarchical Ag-SiO2@Fe3O4 magnetic composites for elemental mercury removal from non-ferrous metal smelting flue gas. Journal of Environmental Sciences. 2019;79:111-20.
23. Kazemnejadi M, Alavi SA, Rezazadeh Z, Nasseri MA, Allahresani A, Esmaeilpour M. Fe3O4@SiO2@Im[Cl] Mn(III)-complex as a highly efficient magnetically recoverable nanocatalyst for selective oxidation of alcohol to imine and oxime. Journal of Molecular Structure. 2019;1186:230-49.
24. Sato T, Masunaga S-i, Kumada H, Hamada N. Microdosimetric Modeling of Biological Effectiveness for Boron Neutron Capture Therapy Considering Intra- and Intercellular Heterogeneity in 10B Distribution. Scientific Reports. 2018;8(1).
25. Wyzlic IM, Tjarks W, Soloway AH, Anisuzzaman AKM, Rong F-G, Barth RF. Strategies for the design and synthesis of boronated nucleic acid and protein components as potential delivery agents for neutron capture therapy. International Journal of Radiation Oncology*Biology*Physics. 1994;28(5):1203-13.
26. Chen W, Mehta SC, Lu DR. Selective boron drug delivery to brain tumors for boron neutron capture therapy. Advanced Drug Delivery Reviews. 1997;26(2-3):231-47.
27. Moss RL. Critical review, with an optimistic outlook, on Boron Neutron Capture Therapy (BNCT). Applied Radiation and Isotopes. 2014;88:2-11.
28. Stöber W, Fink A, Bohn E. Controlled growth of monodisperse silica spheres in the micron size range. Journal of Colloid and Interface Science. 1968;26(1):62-9.
29. Ito Y, Kimura Y, Shimahara T, Ariyoshi Y, Shimahara M, Miyatake S, et al. Disposition of TF-PEG-Liposome-BSH in tumor-bearing mice. Applied Radiation and Isotopes. 2009;67(7-8):S109-S10.
30. Nakamura H, Ueno M, Ban HS, Nakai K, Tsuruta K, Kaneda Y, et al. Development of boron nanocapsules for neutron capture therapy. Applied Radiation and Isotopes. 2009;67(7-8):S84-S7.
31. Zaboronok A, Yamamoto T, Nakai K, Yoshida F, Uspenskii S, Selyanin M, et al. Hyaluronic acid as a potential boron carrier for BNCT: Preliminary evaluation. Applied Radiation and Isotopes. 2015;106:181-4.
32. Trivillin VA, Garabalino MA, Colombo LL, González SJ, Farías RO, Monti Hughes A, et al. Biodistribution of the boron carriers boronophenylalanine (BPA) and/or decahydrodecaborate (GB-10) for Boron Neutron Capture Therapy (BNCT) in an experimental model of lung metastases. Applied Radiation and Isotopes. 2014;88:94-8.
33. Miyabe J, Ohgaki R, Saito K, Wei L, Quan L, Jin C, et al. Boron delivery for boron neutron capture therapy targeting a cancer-upregulated oligopeptide transporter. Journal of Pharmacological Sciences. 2019;139(3):215-22.
34. Shu D, Tang X, Geng C, Zhang X, Gong C, Shao W, et al. Novel method exploration of monitoring neutron beam using Cherenkov photons in BNCT. Radiation Physics and Chemistry. 2019;156:222-30.
35. Heber EM, Trivillin VA, Nigg DW, Itoiz ME, Gonzalez BN, Rebagliati RJ, et al. Homogeneous boron targeting of heterogeneous tumors for boron neutron capture therapy (BNCT): Chemical analyses in the hamster cheek pouch oral cancer model. Archives of Oral Biology. 2006;51(10):922-9.
36. Watabe T, Hanaoka K, Naka S, Kanai Y, Ikeda H, Aoki M, et al. Practical calculation method to estimate the absolute boron concentration in tissues using 18F-FBPA PET. Annals of Nuclear Medicine. 2017;31(6):481-5.
37. Sauerwein W, Moss R, Stecher-Rasmussen F, Rassow J, Wittig A. Quality management in BNCT at a nuclear research reactor. Applied Radiation and Isotopes. 2011;69(12):1786-9.
38. Lee J-C, Chen Y-W, Chuang K-S, Hsu F-Y, Chou F-I, Hsu S-M, et al. The Dosimetric Impact of Shifts in Patient Positioning during Boron Neutron Capture Therapy for Brain Tumors. BioMed Research International. 2018;2018:1-11.
39. Farhood B, Samadian H, Ghorbani M, Zakariaee SS, Knaup C. Physical, dosimetric and clinical aspects and delivery systems in neutron capture therapy. Reports of Practical Oncology & Radiotherapy. 2018;23(5):462-73.
40. Maruyama K, Ishida O, Kasaoka S, Takizawa T, Utoguchi N, Shinohara A, et al. Intracellular targeting of sodium mercaptoundecahydrododecaborate (BSH) to solid tumors by transferrin-PEG liposomes, for boron neutron-capture therapy (BNCT). Journal of Controlled Release. 2004;98(2):195-207.
41. Carpano M, Perona M, Rodriguez C, Nievas S, Olivera M, Santa Cruz GA, et al. Experimental Studies of Boronophenylalanine (10BPA) Biodistribution for the Individual Application of Boron Neutron

Capture Therapy (BNCT) for Malignant Melanoma Treatment. International Journal of Radiation Oncology*Biology*Physics. 2015;93(2):344-52.
42. Woollard JE, Blue TE, Curran JF, Mengers TF, Barth RF. An alpha autoradiographic technique for determination of 10B concentrations in blood and tissue. Nuclear Instruments and Methods in Physics Research Section A: Accelerators, Spectrometers, Detectors and Associated Equipment. 1990;299(1-3):600-5.
43. Hassanein AM, Hassan MH, Mohamed NMA, Abou Mandour MA. An optimized epithermal BNCT beam design for research reactors. Progress in Nuclear Energy. 2018;106:455-64.
44. Marone PA, Heimbach JT, Nemzer B, Hunter JM. Subchronic and genetic safety evaluation of a calcium fructoborate in rats. Food and Chemical Toxicology. 2016;95:75-88.
45. Kanemitsu T, Kawabata S, Fukumura M, Futamura G, Hiramatsu R, Nonoguchi N, et al. Folate receptor-targeted novel boron compound for boron neutron capture therapy on F98 glioma-bearing rats. Radiation and Environmental Biophysics. 2018;58(1):59-67.
46. Musacchio González E, Martín Hernández G. An accelerator-based Boron Neutron Capture Therapy (BNCT) facility based on the 7 Li(p,n) 7 Be. Nuclear Instruments and Methods in Physics Research Section A: Accelerators, Spectrometers, Detectors and Associated Equipment. 2017;865:148-51.
47. Ciani L, Bortolussi S, Postuma I, Cansolino L, Ferrari C, Panza L, et al. Rational design of gold nanoparticles functionalized with carboranes for application in Boron Neutron Capture Therapy. International Journal of Pharmaceutics. 2013;458(2):340-6.
48. Alberti D, Protti N, Toppino A, Deagostino A, Lanzardo S, Bortolussi S, et al. A theranostic approach based on the use of a dual boron/Gd agent to improve the efficacy of Boron Neutron Capture Therapy in the lung cancer treatment. Nanomedicine: Nanotechnology, Biology and Medicine. 2015;11(3):741-50.
49. Gambarini G, Negri A, Regazzoni V, Magni D, Nolli R, Campi F, et al. Methods for dose measurements in small phantoms irradiated at BNCT epithermal column. Applied Radiation and Isotopes. 2014;88:118-24.
50. Ceberg CP, Salford LG, Brun A, Hemler RJB, Persson BRR. Neutron capture imaging of 10B in tissue specimens. Radiotherapy and Oncology. 1993;26(2):139-46.